

# Linear Constraints Learning for Spiking Neurons

Huy Le Nguyen  
hln7@kent.ac.uk

Dominique Chu  
dfc@kent.ac.uk

March 1, 2025

## Abstract

Encoding information with precise spike timings using spike-coded neurons has been shown to be more computationally powerful than rate-coded approaches. However, most existing supervised learning algorithms for spiking neurons are complicated and offer poor time complexity. To address these limitations, we propose a supervised multi-spike learning algorithm which reduces the required number of training iterations. We achieve this by formulating a large number of weight updates as a linear constraint satisfaction problem, which can be solved efficiently. Experimental results show this method offers better efficiency compared to existing algorithms on the MNIST dataset. Additionally, we provide experimental results on the classification capacity of the LIF neuron model, relative to several parameters of the system.

## 1 Introduction

Spiking Neural Networks (SNNs) (Gerstner and Kistler, 2002) have been shown to be computationally more powerful compared to traditional Artificial Neural Networks (Maass, 1997), even on the level of single neurons with single output spikes (Rubin et al., 2010). Though the computational power of SNNs has been demonstrated, practical applications are limited by their complexity. Large models with many parameters and high precision requirements are expensive to simulate and train, thus cannot meet the demands of real-time applications (Querlioz et al., 2013; Diehl and Cook, 2015; Balaji et al., 2020). While there are recent efforts (Yu et al., 2013b; Xu et al., 2018; Yu et al., 2019; Cheng et al., 2020; Li and Yu, 2020) to design smaller architectures which maintain competitive accuracy, it remains a significant challenge to analytically determine what SNN architecture, connectivity, or size are sufficient to enable robust capacity, even on elementary problems. In order to better understand the computational properties of SNNs, more efficient learning methods are required to enable further explorations of the capabilities of individual nodes in a network.

The fundamental computation of single neuron models is the transformation of input signals into a desired output signal, more commonly referred to as the problem of implementing precise input-output associations. In this area, there have been a number of spike-time based methods based on using spike-timings as the supervisory signal. The Remote Supervised Method (ReSuMe) (Ponulak and Kasiński, 2010) is a classic supervised learning method which utilises the biologically plausible STDP mechanisms with the Widrow-Hoff window to modify synaptic efficacy. Recently, first-error based methods (Memmesheimer et al., 2014; Luo et al., 2019) demonstrated an approach where the error signal is the time of the first difference between actual and desired spike trains in each trial. These methods demonstrate robust capacity, but the application of the weight update centered primarily around one spike time results in poor complexity. Yu et al. (2013a) uses all available spike times during learning, but still requires a number of iterations

to modify the output of the neuron to the desired times. Importantly, it is not yet clear how these methods may be applied to problems which do not provide desired spike times as initial conditions.

Recently, membrane-potential based methods emerged as a robust supervised learning approach. Representative examples are the Tempotron (Gütig and Sompolinsky, 2006) and Multi-Spike Tempotron (MST) (Gutig, 2016) algorithms, which are designed to solve binary classification and multi-spike classification problems, respectively. These methods rely on the values of the membrane potential during simulation to derive weight updates in a gradient-descent approach. The MST method has demonstrated the ability to find appropriate output spike times for a given problem, however the complex recursive derivations as well as the requirement to simulate the neuron several times per trial is detrimental to efficiency. The High-Threshold-Projection method (Memmesheimer et al., 2014) takes a different approach to utilising membrane potential values as error signals, based on taking discrete subsamples of membrane potential at error times to solve the precise input-output learning problem. Membrane potential-driven methods have been demonstrated to be theoretically robust for many multi-spike learning problems. However, the complexity of gradient calculations in such methods poses as a constant limiting factor. In recent years, many efforts (Zhang et al., 2018; Miao et al., 2018; Xiao et al., 2019) have gone towards simplifying the required computations of these methods, either by theoretical or numerical approximations.

In summary, while spiking neuron models are computationally powerful, existing methods to train them are plagued by efficiency problems, thus preventing rigorous exploration of computational properties of their underlying models. In this work, we propose a efficient supervised multi-spike learning method. By using a sufficiently simple weight update rule, we can formulate a large number of weight updates as a linear constraint satisfaction problem, which can then be solved efficiently and simultaneously using existing numerical methods. Experimental results show our method is able to converge to solutions in significantly fewer learning iterations compared to existing approaches, for two different multi-spike learning problems. Using this method, we perform an exploration of model parameter spaces to investigate the behaviour of the model at capacity. Experimental results show the LIF model has the ability to simultaneously operate with precision across a large range of output requirements.

## 2 Results

In this work we consider the LIF neuron model for its computational properties and simplicity (Gerstner and Kistler, 2002). The model consists of weighted input channels, an output channel, and an internal state that changes over time. There are  $N$  input channels which receive spike events as inputs. An input spike is a discrete event modelled as a Dirac Delta function  $\delta(t - t_j^i)$  at the  $i$ -th channel at time  $t_j^i \in \mathbb{R}^+$ . The real-valued internal state of the neuron is called the membrane potential. The momentary membrane potential value  $V(t)$  is modelled as:

$$V(t) = V_0(t) - \vartheta \sum_{t_j^s < t} \exp\left(-\frac{t - t_j^s}{\tau_m}\right) \quad (1)$$

$$V_0(t) = \sum_{i=1}^N w_i \sum_{t_j^i < t} K(t - t_j^i) \quad (2)$$

Here,  $t_j^i$  denotes the time of the  $j$ -th input spike of the  $i$ -th input channel, and  $t_j^s$  denotes the time of the  $j$ -th output spike.  $\vartheta = 1$  is the constant spiking threshold. In Equation 2, input spike times are converted to analog membrane potential contribution values, in which channel weights  $w_i$  define the amplitude and the temporal kernel  $K$  defines the shape:

$$K(t - t_i) = V_{\text{norm}} \left( \exp \left( \frac{-(t - t_i)}{\tau_m} \right) - \exp \left( \frac{-(t - t_i)}{\tau_s} \right) \right)$$

$\tau_m$  and  $\tau_s$  are time constants of the membrane potential and synaptic currents, respectively.  $V_{\text{norm}}$  is a normalisation constant:

$$\gamma = \frac{\tau_m}{\tau_s}$$

$$V_{\text{norm}} = \frac{\gamma^{\frac{\gamma}{\gamma-1}}}{\gamma - 1}$$

If  $V(t)$  crosses  $\vartheta$  from below, an output spike is generated (unmodelled), and the time  $t$  is recorded. Each output spike time  $t_j^s$  results in a non-linear reset to the membrane potential after this time, the effect of which is calculated by the sum in Equation 1.

The neuron described above can be viewed as a mapping induced by weights  $w = (w_1, w_2, \dots, w_N)$  which maps from input set  $I$  to output set  $O$ :

$$w : I \rightarrow O \quad (3)$$

Here the input set  $I$  is the set containing all sets of tuples  $t^i := (t \in \mathbb{R}, i \in \mathbb{N})$ , denoting the time  $t$  of an input spike at input channel  $i$  to the neuron. We define an input *pattern* as a specific set of tuples defining a specific sequence of input spikes, denoted as  $x \in I$ . Similarly, the output set  $O$  is a set of sets of spike times of the neuron. Equation 1 does not have a stochastic (noise) part, thus a neuron equipped with some weights  $w$  deterministically performs the mapping  $w : x \mapsto w(x)$ ,  $w(x) \in O$ . Here,  $w(x)$  is a set of output spike times produced by a neuron. If the neuron did not spike in response to  $x$ , then  $w(x) = \emptyset$ . Unless specified otherwise, input patterns are randomly generated, such that each input spike time is generated using a homogeneous Poisson point process with rate  $\nu_{in}$  and duration  $T$ . Once generated, the patterns are always kept fixed for learning.

## 2.1 Learning Precise Input-Output Times

For this learning problem, we are given a fixed input pattern  $x$  and a set of desired output spike times denoted as  $y \in O$ . The problem statement is to find weights  $w$  such that  $w(x) = y$ . By definition of the model dynamics in Equation 1, the neuron with weights  $w$  obeys the following constraints on the membrane potential:

Threshold Equality:  $\vartheta = V(t)$  at all spike times  $t \in w(x)$

Threshold Inequality:  $\vartheta > V(t)$  at all other times

There are a finite number of threshold equality constraints (as  $w(x)$  is finite) and an infinite number of threshold inequality constraints (as time is continuous). Memmesheimer et al. (2014) has shown that in practice, the number of inequalities is effectively finite due to strong temporal correlations in the inputs. This means the number of *relevant* threshold inequalities is always dependent on the current state of the system, *i.e.* the weights. We call this set of relevant timings ‘error’ times, which will be iteratively determined in our algorithm. We now show that using a sufficiently simple learning rule, this learning problem can be formulated as a constraint satisfaction problem with the same dimensionality as the number of threshold constraints.

Our algorithm is an iterative procedure, which starts with the set of desired times  $y$  and an initial value of the set of error times  $e = \emptyset$  (denoting the empty set). While it is not possible to

analytically determine  $e$  at initialisation, our algorithm iteratively interprets the values in this set based on  $w(x)$ . The initial weights  $w^{\text{init}}$  are set to all zero. Then, using a method we call Discrete Threshold Assumption (DTA) we compute  $w$  such that threshold equality constraints are obeyed at times  $y$  and threshold inequality constraints are obeyed at times  $e$ . In this procedure  $V(t)$  is only calculated at  $t \in y$  and  $t \in e$ , thus at any other times the membrane potential may cross the threshold, and *actual* output times  $w(x)$  may still be different to desired times  $y$ . If this is the case, we set  $e = w(x) \setminus y$  for the next DTA iteration. This procedure terminates when (1)  $w(x) = y$ , or (2) the maximum allowed iterations is reached.

To monitor the correctness of solutions throughout learning, we use the correlation-based measure introduced by Schreiber et al. (2003), denoted  $C$ . This metric is calculated after each iteration, as:

$$C = \frac{\overrightarrow{w(x)} \cdot \vec{y}}{|\overrightarrow{w(x)}| |\vec{y}|}$$

Here,  $\overrightarrow{w(x)}$  and  $\vec{y}$  are vectors representing a convolution of  $w(x)$  and  $y$ , respectively.  $\overrightarrow{w(x)} \cdot \vec{y}$  represents the inner product of these vectors, and  $|\overrightarrow{w(x)}|$ ,  $|\vec{y}|$  are their respective Euclidean norms. The convolution is performed using low-pass Gaussian filters of the form

$$G(c, \sigma) = \exp\left(-\frac{t^2}{2\sigma^2}\right)$$

$\sigma$  is the width of the filter, and  $c$  is the filter center. Each convolution filter is centered on discrete time points between 1 and  $T$ , such that  $\vec{y} = [\sum_{a \in y} G(c - a, \sigma)]$  for  $c = 1, 2, \dots, \lfloor T \rfloor$  where  $\lfloor T \rfloor$  is pattern duration  $T$  rounded down to the nearest integer. We set  $\sigma = 20$ , so that the filter is more sensitive to the effects of additional/missing spikes, rather than small differences in spike times. The range of  $C$  is 0 (no correlation) to 1 (identical spike trains).  $C = 1$  is equivalent to the termination condition  $w(x) = y$ .

### 2.1.1 Discrete Threshold Assumption Method

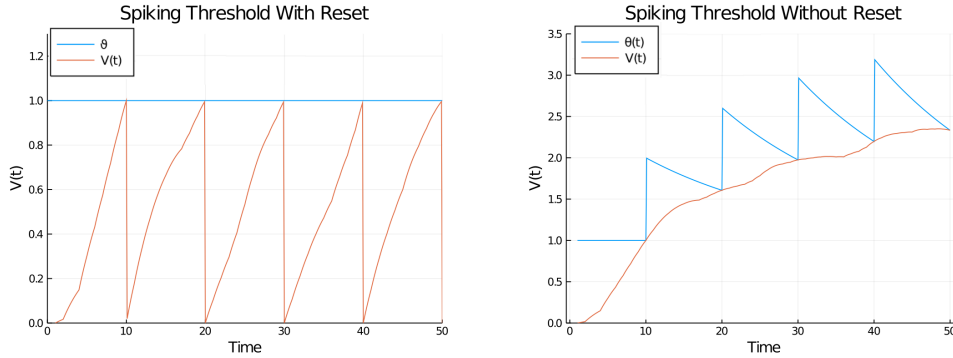


Figure 1: Membrane potential traces (a) with and (b) without ‘soft’ reset of a neuron trained to output spikes at  $y = \{10, 20, 30, 40, 50\}$  in response to a randomly generated pattern. The two approaches result in the same output spikes, however using the membrane potential trace in (b) allows for direct modification of the shape of the membrane potential using only the synaptic contributions.

Given initial weights  $w^{\text{init}}$ , desired output times  $y$ , and error times  $e$ , The DTA method computes updated weights  $w = w^{\text{init}} + \Delta w$  such that the threshold constraints are satisfied:

$$\vartheta = V(t), \text{ for } t \in y \quad (4)$$

$$\vartheta > V(t), \text{ for } t \in e \quad (5)$$

Due to the reset of  $V(t)$  at output times  $y$ , computing input-output correlations w.r.t.  $w$  is difficult. Thus, in the following equations we calculate the membrane potential without reset  $V_0(t)$ , and at each time  $y$  the spiking threshold is non-linearly increased. We denote this spiking threshold as  $\theta$ . The momentary value of  $\theta$  is:

$$\theta(t) = \vartheta + \vartheta \sum_{t^* < t} \exp\left(-\frac{t - t^*}{\tau_m}\right); t^* \in y \quad (6)$$

The sum in Equation 6 is taken over all spike times  $t^* \in y$  which come before  $t$ . Equations 4 and 5 now become:

$$\theta(t) = V_0(t), \text{ for } t \in y \quad (7)$$

$$\theta(t) > V_0(t), \text{ for } t \in e \quad (8)$$

The difference between the constant threshold  $\vartheta$  and non-linear threshold  $\theta$  is demonstrated in Figure 1b. Applying weight updates to  $V_0(t)$  instead of  $V(t)$  removes the complexity of including the non-linear effects of threshold reset while deriving changes to the shape of the membrane potential w.r.t. weights. Substituting Equation 2 into Equations 7 and 8 gives:

$$\theta(t) = \sum_{i=1}^N (w_i^{\text{init}} + \Delta w_i) \sum_{t_i^j < t} K(t - t_i^j), \text{ for } t \in y \quad (9)$$

$$\theta(t) > \sum_{i=1}^N (w_i^{\text{init}} + \Delta w_i) \sum_{t_i^j < t} K(t - t_i^j), \text{ for } t \in e \quad (10)$$

The inner sums above are taken over all input spikes which arrive before  $t$ . To calculate  $\Delta w$ , we use the Tempotron (Gütig and Sompolinsky, 2006) weight update rule:

$$\Delta w_i = \pm \eta \sum_{t_i^j < t} K(t - t_i^j)$$

Here,  $\eta$  is a real-valued learning rate. This equation is commonly used to iteratively increase/decrease weights until a spike is produced/eliminated at time  $t$ . Since the learning rate  $\eta$  is typically very small, this usually requires a large number of weight update iterations. To avoid this computational cost, we propose instead to calculate the *value of the learning rate* that would produce/eliminate an output spike in one update. This means we only calculate  $D = |y| + |e|$  weight updates, one for each desired/undesired spike. For each weight update, we calculate a corresponding learning rate. Thus, we define  $\Delta w_i$  as the sum of  $D$  weight updates:

$$\Delta w_i = \sum_{m=1}^{|y|} \eta_m \sum_{t_i^j < t} K(t_m - t_i^j) + \sum_{n=1}^{|e|} \eta_n \sum_{t_i^j < t} K(t_n - t_i^j) \quad (11)$$

Here,  $t_m$  denotes the  $m$ -th element in  $y$ , and  $t_n$  denotes the  $n$ -th element in  $e$ .  $\eta_m$  is the learning rate value at time  $t_m$ ,  $\eta_n$  is the learning rate at time  $t_n$ . We now have  $D$  linear constraints

of the form in Equations 9 and 10, and  $D$  unknown ‘learning rate’ variables to solve for. We use a linear constraint satisfaction optimizer with the interior-point method to simultaneously solve for all  $\eta_m$  and  $\eta_n$  variables. If unbounded, learning rate values may explode and result in non-sensible solutions. Thus, in addition to the linear threshold constraints, we impose additional boundary constraints  $\eta_m \leq 0.9$  and  $-0.2 \leq \eta_n \leq 0$ , which we find to provide good stability for  $0.005 \leq \nu_{in} \leq 0.04$ . The boundaries must be tuned experimentally: if they are too small, the problem becomes infeasible in variable space. If they are too large, resulting  $w(x)$  will contain many undesired output spikes due to overshoot. Substituting the resulting  $\eta_m$  and  $\eta_n$  values in Equation 11 yields weights  $w = w^{\text{init}} + \Delta w$  which satisfies all threshold constraints given by  $y$  and  $e$ . The solution  $w$  from one iteration is used as  $w^{\text{init}}$  for the next iteration, if convergence is not yet reached.

### 2.1.2 Pattern Memorisation Performance

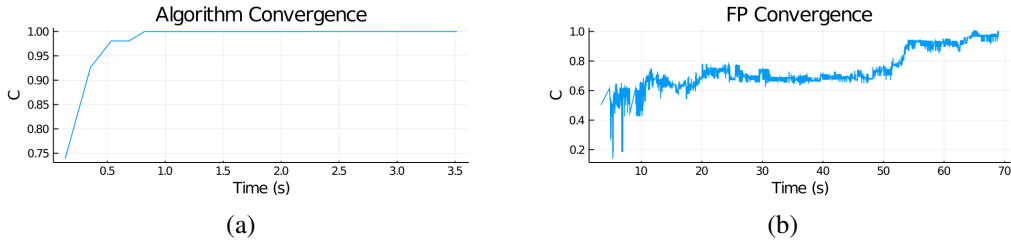


Figure 2: Comparison of convergence behaviour based on correlation metric  $C$  throughout learning of the pattern memorisation task. The proposed method converges to a solution faster and with more stability compared to the FP algorithm.

We benchmark the learning efficiency of our method against the FP method (Memmesheimer et al., 2014). We generate 50 samples of input patterns and desired output sequences, then apply each algorithm. Input patterns are generated with  $N = 500$  afferents, duration  $T = 1000$ , in spiking rate  $\nu_{in} = 0.005$ . Desired output spike sequences are generated using a Poisson point process with rate  $\nu_{out} = 0.01$ . With the FP algorithm, we set the learning precision  $\epsilon = 0.01$ , learning rate  $\lambda = 0.01$ , and maximum iterations = 20000. With the proposed method, we set maximum iterations = 40.

	Final correlation ( $C$ )	Time (s)	Time per iteration (s)
Proposed Method	$0.98 \pm 0.06$	$0.16 \pm 0.20$	$0.013 \pm 0.006$
FP	$0.72 \pm 0.15$	$92.16 \pm 7.78$	$0.0046 \pm 0.0004$

Table 1: Mean and standard deviation of algorithm runtime and accuracy on the pattern memorisation task, averaged over 50 independent trials.

Table 1 shows the runtime and  $C$  value at termination for both algorithms. Results suggest our method is able to converge to a solution faster and more accurately compared to the FP method. The computation time per iteration is an order of magnitude slower than the simple computation done by the FP method, however our method requires significantly fewer learning iterations. With this experimental setup, our method reaches  $C = 0.9$  after only two to three iterations on average. Figure 3 shows the effect of parameters the number of inputs  $N$  and the pattern duration  $T$  on the memorisation performance. Performance gradually increases as the value of  $N$  and  $T$  increases.

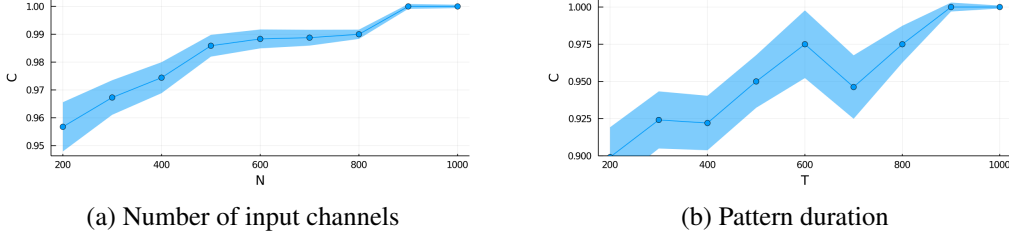


Figure 3: Effects of number of input channels  $N$  and pattern duration  $T$  on the final  $C$  value. Performance increases as the space of available parameters (spatial and temporal) increases. Each data point is averaged over 100 independent trials.

### 2.1.3 Memorisation Capacity

We investigate the maximal capacity of the neuron model to memorise input-output associations. Since numerical results on this matter are already established in Memmesheimer et al. (2014) using their HTP and FP methods, here we use the same benchmark metrics, and only confirm that the improved efficiency of our method does not come at the detriment of the capacity. The capacity is measured in units of  $\tau = \sqrt{\tau_m \tau_s}$  (Rubin et al., 2010), and is defined as the maximal combined duration of the inputs that can be learned, normalised by the number of synapses:  $T_\alpha / N\tau$ .

To measure this, we generate inputs of duration  $T$ , with  $N = 1000$  and  $\nu_{in} = 0.005$ . Output sequences were generated with  $\nu_{out} = 0.001$  or  $0.005$ , normalised over the range  $\tau_m \rightarrow T$ . The biologically plausible ratio  $\tau_m / \tau_s = 4$  is kept constant, and the capacity was measured with different values of  $\tau_m$ . For each data point, the input duration  $T$  is incrementally increased until approximately half of 50 samples failed to converge within 40 iterations. The sum duration of the samples which did not fail to converge is taken as  $T_\alpha$ . Results in Figure 4 indicate our method achieves similar capacity compared to the HTP and FP methods.

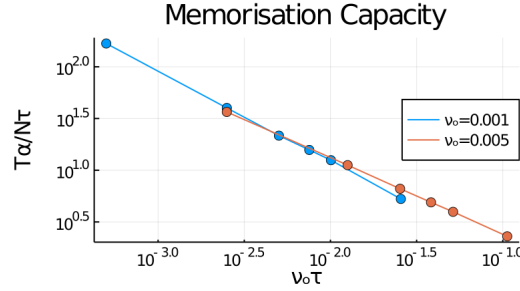


Figure 4: Capacity of LIF neuron on the pattern memorisation task. Data points (from left to right) of each series are trials with  $\tau_m = \{1.0, 5.0, 15.0, 20.0, 50.0\}$ , which is used to calculate  $\nu_{out}\tau$  on the x-axis. This data demonstrates similar capacity to Memmesheimer et al. (2014)

## 2.2 Classification with Unknown Spike Times

For this task, there are multiple input patterns, and with some modification to the DTA method we show that the neuron can learn to classify the input patterns into different classes. We generate  $P$  random input patterns and assign to each pattern a positive integer label. We use  $x_p$ ,  $l_p$ , and  $w(x_p)$  to respectively denote the  $p$ -th input pattern, its label, and the neuron's output response to this input. We define classification of  $x_p$  as the number of spikes  $|w(x_p)|$  that the neuron outputs in response. One generated, the patterns and their labels are kept fixed for learning. The pattern classification problem is calculating weights  $w$  which satisfies the condition:

$$|w(x_p)| = l_p, \text{ for all } p \quad (12)$$

Unlike the pattern memorisation task, the output spike times  $y_p$  which solves this task are initially unknown. Thus, the problem is equivalent to finding appropriate output spike times for each pattern, for which a solution exists.

### 2.2.1 Determining Output Times

To find output spike times  $y_p$  and error spike times  $e_p$  for each weight update iteration, we use a dynamic threshold process (Gutig, 2016; Yu et al., 2019). The process can be summarised as follows: by simulating the neuron with a different threshold value to the constant threshold  $\vartheta$ , we may obtain a set of output spike times with more or fewer output spikes, the timings of which can then be used as ‘desired’ output spike times  $y_p$  for threshold equality constraints.

Here, we extend the notation  $w(x_p)$  to  $w(\vartheta^*, x_p)$  to denote the set of output spike times elicited by a neuron equipped with weights  $w$ , processing the input  $x_p$  using a real-valued threshold  $\vartheta^*$  in Equation 1. Generally, by simulating the neuron with a lower spiking threshold ( $\vartheta^* < \vartheta$ ), there will be more output spikes; with  $\vartheta^* > \vartheta$  there will be fewer output spikes.

Thus, we first simulate the neuron with  $x_p$  to obtain  $w(\vartheta, x_p)$ . Then, for each  $x_p$  we determine a corresponding threshold value  $\vartheta_p^*$  such that:

- If  $|w(\vartheta, x_p)| < l_p$ , then  $\vartheta^*$  satisfy  $|w(\vartheta^*, x_p)| = |w(\vartheta, x_p)| + 1$
- If  $|w(\vartheta, x_p)| > l_p$ , then  $\vartheta^*$  satisfy  $|w(\vartheta^*, x_p)| = |w(\vartheta, x_p)| - 1$

We determine appropriate values for  $\vartheta_p^*$  by interval halving in the interval  $(0, 10\vartheta)$  until one of the above conditions are fulfilled. Then, we set  $y_p = w(\vartheta_p^*, x_p)$ , and  $e_p = w(\vartheta, x_p) \setminus w(\vartheta_p^*, x_p)$  for use in the weight update equation (presented below).

### 2.2.2 DTA-Classification

Here, we present the changes to the equations in Section 2.1.1 to make the DTA method suitable for classification. Equations 4 to 10 are computed at times  $y_p$  and  $e_p$  instead of  $y$  and  $e$ , respectively. The main impact is that the threshold function  $\theta(t)$  (Equation 6) will have a different shape for each pattern, depending on the times  $y_p$  used to calculate Equation 6.

Since there are  $P$  input patterns, the dimensionality of the constraint satisfaction problem becomes  $D = \sum_{p=1}^P (|y_p| + |e_p|)$ . The total weight change  $\Delta w$  (Equation 11) now requires an additional sum:

$$\Delta w_i = \sum_{p=1}^P \left( \sum_{m=1}^{|y_p|} \eta_{p,m} \sum_{t_j^i < t} K(t_{p,m} - t_j^i) + \sum_{n=1}^{|e_p|} \eta_{p,n} \sum_{t_j^i < t} K(t_{p,n} - t_j^i) \right) \quad (13)$$

Here,  $t_{p,m}$  denotes the  $m$ -th element in  $y_p$ , and  $t_{p,n}$  denotes the  $n$ -th element in  $e_p$ .  $\eta_{p,m}$  is the learning rate value at time  $t_{p,m}$ ,  $\eta_{p,n}$  is the learning rate at time  $t_{p,n}$ . The system is solved using a linear constraint optimizer as in Section 2.1.1, using the same variable bounds.

### 2.2.3 DTA Convergence Behaviour

Here, we explore the convergence behaviour of the DTA methods with respect to parameters  $\tau_m$ , the constant threshold  $\vartheta$ , the number of input afferents  $N$ , and the input spiking rate  $\nu_{in}$ . Other than the independent variables, the parameter setup is  $\tau_m = 20.0, \tau_m/\tau_s = 4, \vartheta = 1, N =$



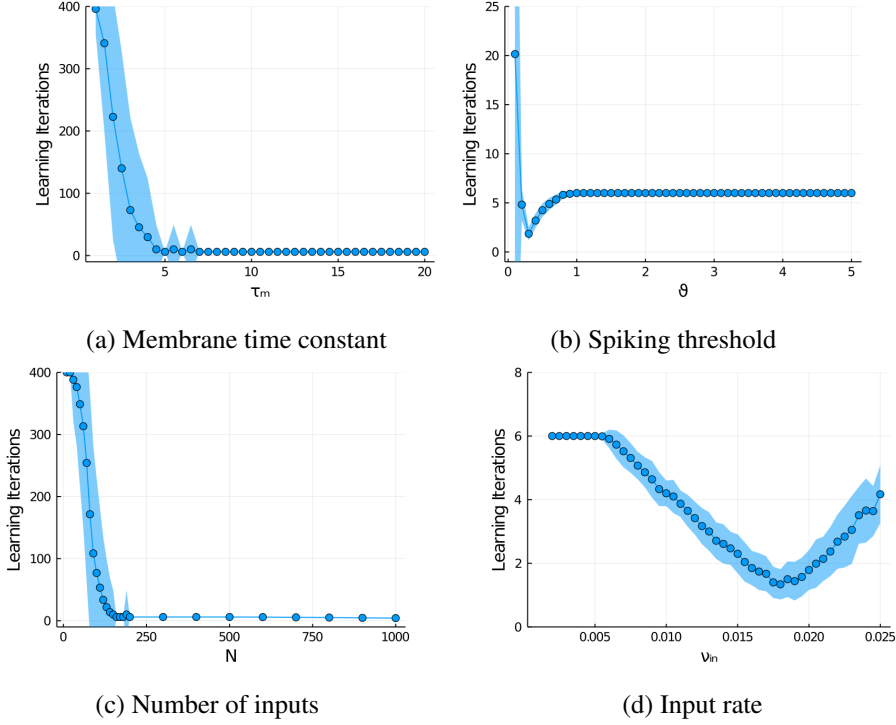


Figure 5: Number of training iterations to convergence using the DTA classification method with various parameter values. Ribbons are standard deviations. Each data point is averaged over 100 independent trials. Above capacity, training time tends towards infinity as there exists no solutions to converge to. Below capacity, the proposed method demonstrates linear time complexity with respect to the sum number of output spikes required by the pattern classification task, constant time complexity with respect to other parameters.

500,  $\nu_{in} = 0.005$ . For 100 independent trials, we generate one input pattern with label 5, and train the neuron for maximum 400 iterations.

Results in Figure 5 indicate the algorithm exhibit linear time complexity with respect to the number of output spikes in the labels, and constant time complexity with respect to other parameters. For data points at capacity (no solutions exist) the number of learning iterations quickly tends towards the maximum iterations. Below capacity, learning converges in 6 iterations with zero variance for all parameters except the input rate  $\nu_{in}$ . For certain ranges of  $\nu_{in}$ , learning starts with a number of output spikes already close to the label, thus requiring fewer than 6 iterations to converge. Interestingly, in more traditional learning algorithms with fixed learning rate parameter, the number of learning iterations should scale linearly with  $\vartheta$  (Xiao et al., 2019). However, the DTA method exhibits constant complexity scaling, due to the adaptive ‘learning rate’ variables  $\eta_{p,m}$  and  $\eta_{p,n}$ .

#### 2.2.4 Classification Performance

We investigate the capability of the DTA-Classification algorithm on the random pattern classification task, compared to the MST method (Gutig, 2016). We generate  $P$  input patterns, and the label for each pattern is randomly assigned between 1 and 5. The pattern size is  $N = 500, T = 50$ , with firing rate  $\nu_{in} = 0.005$ . We compare the runtime and classification accuracy of our algorithm with that of the MST algorithm for various dataset sizes  $1 \leq P \leq 100$ . Each data point is averaged over 30 independent trials.

Neurons trained with MST are trained for a maximum of 200 training cycles of 100 iterations each (20000 iterations total), with learning rate  $\eta = 0.001$  and momentum parameter  $\mu = 0.5$ . Neurons trained with DTA are trained for the same number of cycles and iterations. All neurons terminate learning early if an entire training cycle has zero classification error.

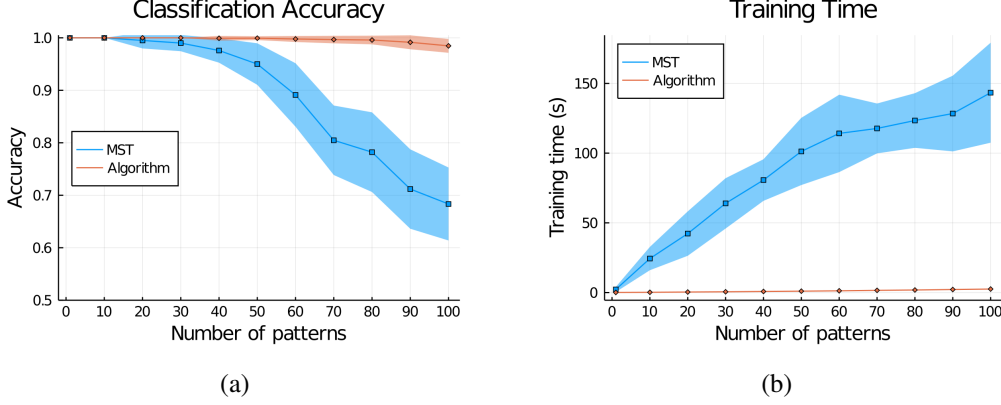


Figure 6: Comparison between the MST algorithm and our algorithm for (a) classification accuracy and (b) training time. Ribbons are standard deviations. Each data point is averaged over 30 independent trials.

Figure 6 shows the accuracy and runtime comparison for the random classification task. At  $P < 60$ , both algorithms achieved perfect (or close to perfect) accuracy on the input patterns, and our algorithm is significantly faster than MST. At  $P = 50$ , our algorithm fully learns the input patterns after 1.01 seconds, compared to the MST average of 101.23 seconds. At  $P = 60$  and above, MST-trained samples stopped showing significant increase in computation time, instead their classification accuracy dropped below 90%. This suggests the MST algorithm can no longer reliably learn the training patterns under these experimental conditions, and a direct comparison becomes less straightforward. At  $P = 100$  input patterns, our algorithm averages 98.5% classification accuracy after 2.46 seconds of runtime, compared to the MST average of 68.3% after 143.35 seconds.

Additionally, we investigate the robustness of the DTA algorithm against input noise (spike jitter) and synaptic (weight) noise. We trained a neuron on a dataset of 5 input patterns, labelled randomly between 1 and 5. For spike jitter, each input pattern is then used as a template to generate ‘noisy’ samples using a Gaussian noise filter with variance value  $\sigma$ . For each  $\sigma$ , we generate  $5 \times 10000$  noisy samples. We then test the classification accuracy of the neuron on all noisy samples and report the average, shown in Figure 7a. Additionally, we also apply the Gaussian filter to each synaptic weight value, also averaging 10000 samples, shown in Figure 7b. Results indicates solutions can tolerate a degree of spike jitter and synaptic noise.

### 2.2.5 Classification Capacity

Using the DTA classification method, we investigate the maximal capacity of the LIF neuron in the random pattern classification task. We define this capacity as the maximum number of classes (denoted  $P_\alpha$ ) which can be distinguished by a single neuron. For simplicity, we consider each class to have only one pattern, and the class labels fill the integer range  $1 \rightarrow P_\alpha$ . Thus, we want to investigate the limiting factors of learning to classify when the disparity between class labels is large, with some patterns requiring few output spikes and others requiring many. We explore how the parameters of the system — in particular  $N$  and  $T$  — affect this capacity.

The experimental setup is as follows: Each sample starts with an empty dataset, and input

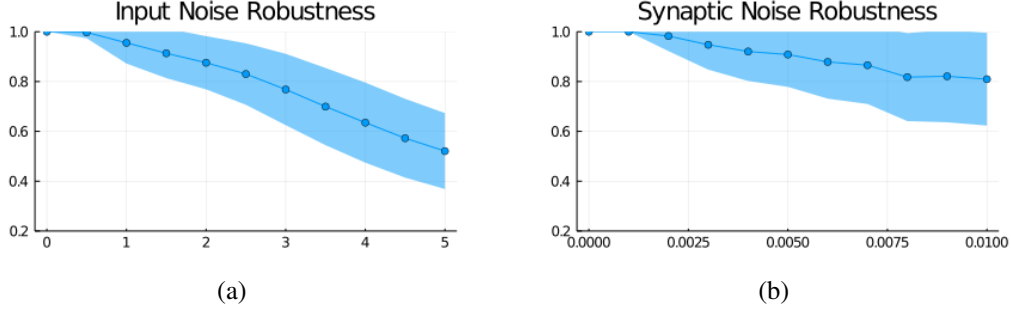


Figure 7: Algorithm performance against varying levels of (a) input noise (b) synaptic (weight) noise. Ribbons are standard deviations. In (b),  $\sigma = 0.01$  is of the same order of magnitude as the mean weight value of solutions ( $\overline{w_i} = 0.02$ ), which represents a high level of synaptic noise.

patterns are incrementally added, where the  $i$ -th pattern is labelled  $i$ . Patterns are added until the neuron can no longer converge to a solution within 100 training cycles, at which point the sample terminates. We take  $P_\alpha$  as the largest number of classes with which at least half of 50 trials can converge to a solution, under a given parameter setup. With the MST method, the sheer number of simulations required by this classification task is prohibitive. With the efficiency of our method, the problem becomes more tractable.

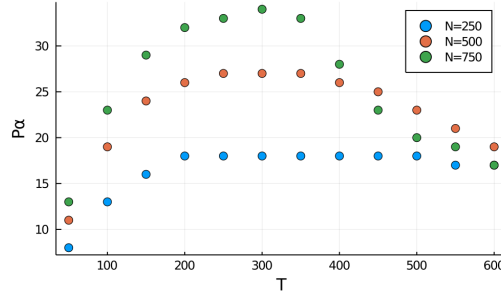


Figure 8: Capacity of LIF neuron in the pattern classification task, with regards to  $T$ . The capacity is higher in the large  $N$  limit, however exhibits enhanced sensitivity to  $T$ , with a smaller range of  $T$  maximising capacity as  $N$  increases.

From Figure 4, we see that the memorisation capacity is a monotonic function of  $\tau_m$ . In this classification scenario, we find that the capacity is instead a non-monotonic concave function of  $\tau_m$ , in which the range  $3 \leq \tau_m \leq 8$  maximises  $P_\alpha$ . This behaviour is consistent with Rubin et al. (2010): if  $\tau_m$  is too small then each output spike is integrated over very few input spikes, leading to larger weights thus more difficult for patterns with small labels to remain quiescent. If  $\tau_m$  is too large, then spike integration happens over a very long period thus it is more difficult to output enough spikes for patterns with large labels, during the time period of the input.

With regards to the pattern duration  $T$ , the capacity also exhibits non-monotonic behaviour, with a small range over  $T$  giving the maximal capacity. The capacity-maximising range of  $T$  exhibit sensitivity to  $N$ , in particular this range becomes smaller as  $N$  increases. To explain why the capacity decreases at the large  $T$  limit, we make an observation of why trials fail here. At large  $T$ , the model consistently fails to classify patterns with smaller labels, always with more spikes than desired. This suggests that the long periods where the neuron must remain quiescent to satisfy small labels is an important limiting factor. In order to classify patterns with larger labels, the synaptic weights must grow to a certain scale, which in turn increases the probability of additional unwanted spikes during patterns with small labels.

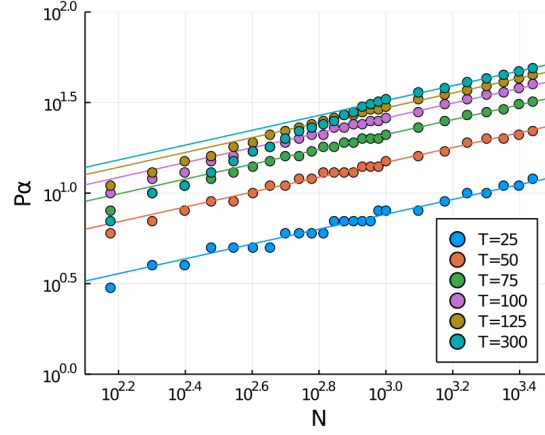


Figure 9: Capacity of LIF neuron in the pattern classification task, with regards to  $N$ . At the large  $N$  limit, the capacity can be approximated by a monomial with exponent  $\approx 0.4$ .

We find the capacity has a positive logarithmic relationship with respect to parameters  $N$ ,  $\nu_{in}$ , and  $\tau_m/\tau_s$  in our results. Refer to Appendix A for results regarding  $\nu_{in}$  and  $\tau_m/\tau_s$ . In the large  $N$  limit, we find the capacity is a monomial, which we estimate as  $P_\alpha = zN^{0.4}$ , and  $z$  is a function of  $T$ . At  $N < 1000$ ,  $P_\alpha$  begins to deviate from this estimate, and with larger values of  $T$  we observe significantly larger deviations. These results are surprising, as each additional class in the dataset defines a different requirement of output statistics, and yet the LIF model demonstrates a robust capacity to operate with precision across a wide range of output regimes, even as the pattern duration  $T$  is finite.

### 2.2.6 Real-world Classification Task

In this section, we demonstrate the performance of the DTA method for solving a realistic image recognition task using a small network of spiking neurons. We use the MNIST dataset for our evaluation. The MNIST dataset consists of images with size  $28 \times 28$  pixels, split into ten classes labelled from 0 to 9 (LeCun and Cortes, 2010). For training and testing, we use the full MNIST data of 60000 train and 10000 test images. To build the network, we use a hybrid feed-forward framework proposed in (Xu et al., 2018) called CSNN, which combines a traditional Convolutional Neural Network (CNN) with a SNN classifier. We compare our results with the EMLC algorithm (Li and Yu, 2020), which is a state-of-the-art membrane-potential based learning method. The architecture has two layers of rate-coded neurons, and two layers of spiking neurons. Computation through the network can be decomposed into three parts: feature extraction, temporal encoding, and classification.

The CNN part is the foremost of the network, which provides feature extraction capabilities. The CNN only has three layers: a convolutional layer (6C5), a max-pooling layer (2P2), and a fully connected output layer with 10 neurons. We train this CNN using traditional backpropagation for 30 epochs, then the CNN parameters are fixed and the output layer discarded. The resulting partial-CNN model performs extraction of invariant local feature maps from the input image, which has been suggested to mimic processes in biology (Xu et al., 2018).

To encode the feature maps produced by the above partial-CNN, the real-valued activations of the pooling layer are linearly mapped to spike times in a time window of length  $T = 100$ . For our CNN architecture, the pooling layer feature maps are flattened to a vector of 864 activation values. We denote the  $i$ -th activation value  $A_i$  and the corresponding spike time  $t_i^{spike}$ . Encoded spike times are calculated as  $t_i^{spike} = T - T \cdot A_i$ . These timings are then used as spike times for the

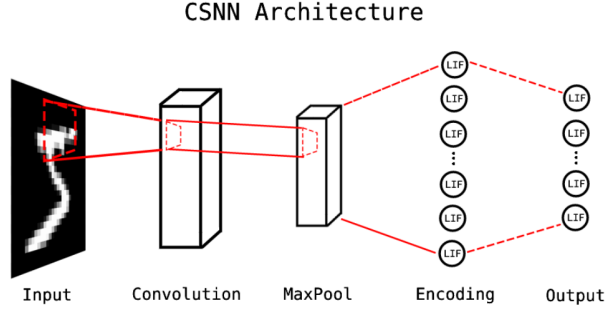


Figure 10: Overview of the CSNN architecture (Xu et al., 2018). The Convolution and MaxPool layers are composed of rate-coded neurons, while the Encoding and Output layers are composed of spiking (LIF) neurons. In our setup, the Encoding layer has 864 neurons and the Output layer has 10 neurons.

encoding layer of LIF neurons. Additionally, any encoding neurons with spike time  $t_i^{spike} = T$  (corresponds to  $A_i = 0$ ) do not spike, as their activation is considered too low to induce input spikes.

The encoding layer is fully connected to the classification layer, which consists of ten LIF neurons to be trained. Each neuron is responsible for recognising a ‘target’ class which it should respond to with 10 output spikes (as in Li and Yu (2020)), and remain quiescent for all other classes. Finally, a Winner-Take-All scheme is applied to the output layer, where the neuron with the highest number of output spikes is chosen as the winner.

To evaluate the performance of the proposed method, we train the above CSNN using the DTA method, the MST method, and the EMLC method. We train CNN-MST and CNN-EMLC over 30000 iterations with learning rate  $\eta = 0.001$  and momentum term  $\mu = 0.9$ . We train CNN-DTA over 5000 iterations.

Method	Time (s)	Train accuracy (%)	Test accuracy (%)
CNN-MST	$856.30 \pm 49.97$	$88.98 \pm 3.52$	$87.59 \pm 4.45$
CNN-EMLC	$656.62 \pm 53.40$	$91.51 \pm 0.16$	$92.26 \pm 0.28$
CNN-DTA	$92.97 \pm 3.85$	$92.72 \pm 0.24$	$92.51 \pm 0.25$

Table 2: Performance comparison of CSNN trained with the MST, EMLC, and DTA methods on the MNIST dataset. Each data point is averaged over 10 independent trials.

The results are shown in Table 2 and Figure 11, and demonstrates significant performance improvements of the DTA method compared to the MST and EMLC methods. Most importantly, the number of training trials required to reach a reasonable degree of accuracy on the test set is much fewer. With the EMLC method, the CSNN model reaches 90% accuracy after approximately 15000 iterations (15000 random training images). In comparison, models trained using the DTA method reach 90% accuracy after only 2500 iterations. This result is important, as reducing the number of learning trials affect CPU time for learning, as well as the (significant) computing requirements for simulating the feature extraction and temporal encoding parts of the CSNN. While the final test accuracy in Table 2 is lower compared to larger architectures such as Diehl and Cook (2015); Cheng et al. (2020), we view this as a current limitation of the CSNN framework itself.

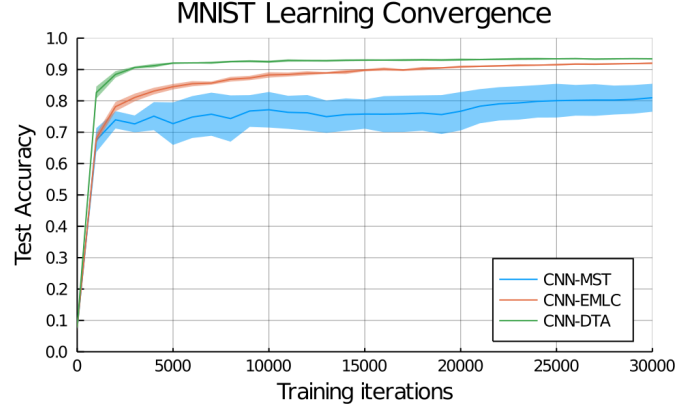


Figure 11: Convergence behaviour of CSNNs trained using different methods on the MNIST task. The proposed DTA method converges to a solution faster and with less variance compared to MST or EMLC. Data shows accuracy on test set over the course of training, averaged over 10 independent trials. Ribbons are standard deviations.

### 3 Discussion

The improved efficiency of our method is due to two novel properties. Firstly, instead of relying on a fixed learning rate or a global adaptive learning rate, the method proposes to calculate an adaptive learning rate *for each update spike time*. This means the process of learning complex spatio-temporal correlations can be done in very few iterations compared to existing approaches, without sacrificing capacity or accuracy. Secondly, the form of Equation 13 and the use of linear constraint optimisation enable the calculation of a multi-spike learning curve applicable to a batch (or mini-batch) of patterns, each with different output requirements. In comparison, many multi-spike learning methods (Gutig, 2016; Diehl and Cook, 2015; Li and Yu, 2020; Xu et al., 2018; Luo et al., 2019) still present input patterns sequentially. To make our results more directly comparable with existing approaches, in Sections 2.2.4 and 2.2.6 we only present one input pattern each iteration. However, in Section 2.2.5 the neuron is presented with the complete dataset at each iteration. This has implications for parallel computing, as all calculations before the linear constraint optimisation step concern independent input patterns, and thus can be performed in parallel.

In this work, we show that properties of existing spike-time based methods and membrane-potential based methods can be combined to form an efficient multi-spike error function. Equations 11 and 13 are fundamentally an interpretation of the Widrow-Hoff window similar to other methods utilising only the spike time as the error signal (Ponulak and Kasiński, 2010; Yu et al., 2013a; Memmesheimer et al., 2014), but with the addition of adaptive learning rate variables. The dynamic threshold process in Section 2.2.1 is similar to how existing methods incorporate membrane potential values in the error signal (Gutig, 2016; Xiao et al., 2019; Yu et al., 2019; Li and Yu, 2020), but without strict precision requirements. In principle, the proposed error function may be extended to train deep or recurrent architectures using techniques which propagate error gradients based on the Widrow-Hoff window, such as Wang et al. (2016); Lin and Shi (2018); Lin and Du (2020). The missing component is how to correctly incorporate the proposed adaptive ‘learning rate’ variables in such methods, which we leave to future work.

An important point to consider in this method is the feasibility of solutions throughout learning. As the number of linear constraints increase, the size of the region containing feasible solutions decreases. When deriving learning algorithms, we often assume that a solution exists according to the formulated problem. This can be advantageous, for example in Section 2.2.5 we use this as an early indicator of failure to converge. However, a disadvantage of this assumption in

the pattern memorisation task is there is no definite way to proceed when the problem is infeasible, other than continue to the next iteration or random minibatch. A potential solution to this problem is a revised first-error approach: only present one constraint initially, then iteratively reintroduce the other constraints back to the system.

## 4 Conclusion

We propose a simple supervised multi-spike learning method based on formulating a large number of weight updates as a linear constraint satisfaction problem, which can be solved in one step. This method greatly reduces the number of update iterations, which in turn reduces the computation time. Experimental results show that our algorithm is capable of solving multi-spike learning problems with improved efficiency, while maintaining comparable capacity to existing approaches. Using this method, we explore the parameter space of the model. Results show LIF neurons are able to simultaneously operate with high precision in a large number of output regimes.

## References

- Balaji, A., Catthoor, F., Das, A., Wu, Y., Huynh, K., Dell’Anna, F. G., Indiveri, G., Krichmar, J. L., Dutt, N. D., and Schaafsma, S. (2020). Mapping spiking neural networks to neuromorphic hardware. *IEEE Transactions on Very Large Scale Integration (VLSI) Systems*, 28:76–86.
- Cheng, X., Hao, Y., Xu, J., and Xu, B. (2020). Lisnn: Improving spiking neural networks with lateral interactions for robust object recognition. *Proceedings of the Twenty-Ninth International Joint Conference on Artificial Intelligence*.
- Diehl, P. U. and Cook, M. (2015). Unsupervised learning of digit recognition using spike-timing-dependent plasticity. *Frontiers in Computational Neuroscience*, 9.
- Gerstner, W. and Kistler, W. M. (2002). *Spiking Neuron Models Single Neurons, Populations, Plasticity*. Cambridge University Press.
- Gütig, R. and Sompolinsky, H. (2006). The tempotron: a neuron that learns spike timing-based decisions. *Nature Neuroscience*, 9:420–428.
- Gutig, R. (2016). Spiking neurons can discover predictive features by aggregate-label learning. *Science*, 351:aab4113–aab4113.
- LeCun, Y. and Cortes, C. (2010). MNIST handwritten digit database. <http://yann.lecun.com/exdb/mnist/>.
- Li, S. and Yu, Q. (2020). New efficient multi-spike learning for fast processing and robust learning. *Proceedings of the AAAI Conference on Artificial Intelligence*, 34:4650–4657.
- Lin, X. and Du, P. (2020). Spike-train level unsupervised learning algorithm for deep spiking belief networks. In Farkaš, I., Masulli, P., and Wermter, S., editors, *Artificial Neural Networks and Machine Learning – ICANN 2020*, pages 634–645, Cham. Springer International Publishing.
- Lin, X. and Shi, G. (2018). A supervised multi-spike learning algorithm for recurrent spiking neural networks. In Kůrková, V., Manolopoulos, Y., Hammer, B., Iliadis, L., and Maglogiannis, I., editors, *Artificial Neural Networks and Machine Learning – ICANN 2018*, pages 222–234, Cham. Springer International Publishing.

- Luo, X., Qu, H., Zhang, Y., and Chen, Y. (2019). First error-based supervised learning algorithm for spiking neural networks. *Frontiers in Neuroscience*, 13.
- Maass, W. (1997). Networks of spiking neurons: The third generation of neural network models. *Neural Networks*, 10:1659–1671.
- Memmesheimer, R.-M., Rubin, R., Ölveczky, B. P., and Sompolinsky, H. (2014). Learning precisely timed spikes. *Neuron*, 82:925–938.
- Miao, Y., Tang, H., and Pan, G. (2018). A supervised multi-spike learning algorithm for spiking neural networks. *2018 International Joint Conference on Neural Networks (IJCNN)*.
- Ponulak, F. and Kasiński, A. (2010). Supervised learning in spiking neural networks with resume: Sequence learning, classification, and spike shifting. *Neural Computation*, 22:467–510.
- Querlioz, D., Bichler, O., Dollfus, P., and Gamrat, C. (2013). Immunity to device variations in a spiking neural network with memristive nanodevices. *IEEE Transactions on Nanotechnology*, 12:288–295.
- Rubin, R., Monasson, R., and Sompolinsky, H. (2010). Theory of spike timing-based neural classifiers. *Physical Review Letters*, 105.
- Schreiber, S., Fellous, J., Whitmer, D., Tiesinga, P., and Sejnowski, T. (2003). A new correlation-based measure of spike timing reliability. *Neurocomputing*, 52-54:925–931.
- Wang, X., Lin, X., Zhao, J., and Ma, H. (2016). Supervised learning algorithm for spiking neurons based on nonlinear inner products of spike trains. In Huang, D.-S. and Jo, K.-H., editors, *Intelligent Computing Theories and Application*, pages 95–104, Cham. Springer International Publishing.
- Xiao, R., Yu, Q., Yan, R., and Tang, H. (2019). Fast and accurate classification with a multi-spike learning algorithm for spiking neurons. *Proceedings of the Twenty-Eighth International Joint Conference on Artificial Intelligence*, pages 1445–1451.
- Xu, Q., Qi, Y., Yu, H., Shen, J., Tang, H., and Pan, G. (2018). Csn: An augmented spiking based framework with perceptron-inception. *Proceedings of the Twenty-Seventh International Joint Conference on Artificial Intelligence*.
- Yu, Q., Li, H., and Tan, K. C. (2019). Spike timing or rate? neurons learn to make decisions for both through threshold-driven plasticity. *IEEE Transactions on Cybernetics*, 49:2178–2189.
- Yu, Q., Tang, H., Tan, K. C., and Li, H. (2013a). Precise-spike-driven synaptic plasticity: Learning hetero-association of spatiotemporal spike patterns. *PLoS ONE*, 8:e78318.
- Yu, Q., Tang, H., Tan, K. C., and Li, H. (2013b). Rapid feedforward computation by temporal encoding and learning with spiking neurons. *IEEE Transactions on Neural Networks and Learning Systems*, 24:1539–1552.
- Zhang, Y., Geng, T., Zhang, M., Wu, X., Zhou, J., and Qu, H. (2018). Efficient and robust supervised learning algorithm for spiking neural networks. *Sensing and Imaging*, 19.



## A Parameter Plots for Classification Capacity

In Section 2.2.5 we focused primarily on parameter interactions between  $T$  and  $N$ . Here, we provide data relating to other parameters of the system affect the maximal classification capacity. Other than the parameter acting as the independent variable in each experiment, control parameter values are  $N = 500$ ,  $T = 50$ ,  $\nu_{in} = 0.005$ ,  $\tau_m = 20.0$ ,  $\tau_m/\tau_s = 4$ .

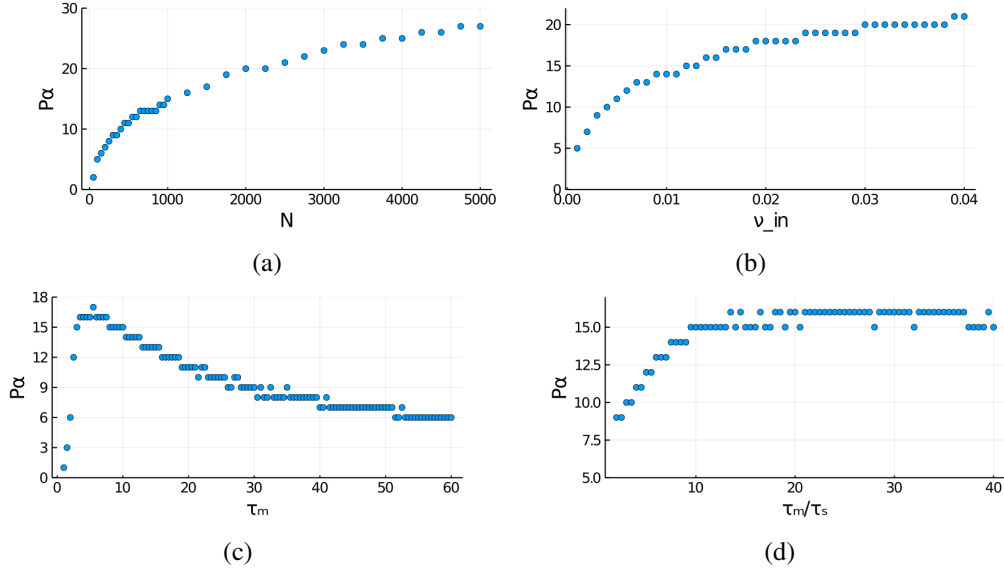


Figure 12: Capacity of LIF neuron in the pattern classification task, with regards to (a) number of input channels  $N$  (same as Figure 9, but with linear axes), (b) input spiking rate  $\nu_{in}$ , (c) membrane time constant  $\tau_m$ , (d) the ratio between  $\tau_m$  and  $\tau_s$ .